BODY SETS AND LINES: A RELIABLE REPRESENTATION OF IMAGES

Michèle Gouiffès and Bertrand Zavidovique

Institut d'Electronique Fondamentale CNRS UMR 8622, University of Paris 11, 91405 ORSAY cedex

ABSTRACT

This paper proposes a novel definition of color lines and sets, based on the dichromatic model for lambertian objects. The ends of the *body vectors* are robustly detected, from the clearest to the darkest through to a multi-level 2D histogram analysis. Finally, instead of classically defining the topographic map along one sole luminance direction, our *body lines* are designed along each body vector. Compared to existing topographic maps, our method is more compact while better preserving the color quality. Furthermore, it is faster to compute than [1].

Index Terms— Image color analysis, color, image segmentation, feature extraction, morphological operations.

1. INTRODUCTION

Most image processing techniques require to reduce, beforehand, the amount of data to be processed. However, the purpose can be quite different from one application domain to another. For data compression purposes, the reduction has to be hardly perceived by the human visual system. In computer vision domain however, images usually need to be reduced to an optimal set of primitives, which have to be both salient and robust to the scene geometry changes, in order to be correctly matched, tracked, interpreted, etc.

Level sets [2] are reputed to convey the most relevant information of an image. Their boundaries, called level lines, are more stable than edges under uniform contrast changes, since they are based on relative intensities. Consequently, they have been exploited for various issues: extraction of meaningful boundaries [3], segmentation [4], robust image registration or matching [5].

Considering the qualities of these primitives, we are interested in studying their extension to color, expecting obvious benefits in robustness and separability. Our present work proposes a novel version of the topographic map [1], more compact and less time-consuming while better preserving the quality and the information of the image.

The continuation of the paper is structured as follows. Section 2 recalls the principles of the existing level sets and lines. Then, Section 3 details our body color lines. To conclude, Section 4 asserts the relevance of the proposed method by comparing it with existing techniques.

2. EXISTING LEVEL SETS AND LINES

Let I(p) be the image intensity at pixel p. I can be decomposed into upper level sets \mathcal{N}^u or lower level sets $\mathcal{N}^l[2]$:

$$\mathcal{N}^u(\mathcal{E}) = \{ p, I(p) \ge \mathcal{E} \}; \quad \mathcal{N}^l(\mathcal{E}) = \{ p, I(p) \le \mathcal{E} \}$$
 (1)

 \mathcal{E} refers to the considered level: $\mathcal{E} \in [0...2^{nb}-1]$, for an image coded on nb digits. The level lines are defined as the boundaries of the level sets. They form a set of Jordan curves which provides a comprehensive description of the image also called the topographic map. Because of the inclusion properties of level sets, level lines do never overlay or cross.

While the gray scale is totally and well ordered, it is obviously more difficult to sort the components of the 3D color space, while trying to preserve the gray lines properties, namely completeness, inclusion and contrast invariance.

In [6] and [7], the authors design the lines in the HSV space, less correlated than RGB and better fitting the human perception. In [6] in particular, colors are totally ordered in a lexicographic fashion by favoring intensity first, then hue and saturation, in order to imitate the perception rules of the human visual system. Unfortunately, they do not take into account the specificities of the HSV space, *i.e* the fact that hue is ill-defined for low saturation.

Defining color sets directly in the RGB space is one solution to answer this problem of noise sensitivity, as in [1]. These results are quite satisfying regarding compactness and quality but the technique is time and resources consuming (several labeling stages, in both image and color space), which is dissuasive for real-time computer vision applications. As [1], our topographic map relies on the dichromatic model.

3. BODY COLOR SETS AND LINES 3.1. Principles

The Shafer dichromatic model [8] states that any inhomogeneous dielectric material, uniformly colored and dull, reflects light by *specular reflection* and *body reflection*. Owing to that model, the colors of a material are distributed in the RGB space according to the coordinates of the *illuminant color* c_s , and the *body color* c_b in a L-shape cluster [9]. For lambertian

space according to the coordinates of the *illuminant color* $\mathbf{c_s}$, and the *body color* $\mathbf{c_b}$ in a L-shape cluster [9]. For lambertian objects however, there is no specular reflection. The colors result directly from the penetration of the light beams into the material, and from its scattering by the pigments. According





Fig. 1. Examples of a color image PARROTS with its color distribution in the RGB space (ColorSpace Software, available on http://www.couleur.org). The body vectors are perfectly visible.

to the dichromatic model, they are roughly located along a finite number of straight lines in the RGB space, *i.e* along each *body vector* going from the black to c_b . Similarly, for faintly saturated images, colors are distributed along the luminance direction. As an example, Fig.1 shows a example of Kodak image PARROTS with the representation of its colors in the RGB space.

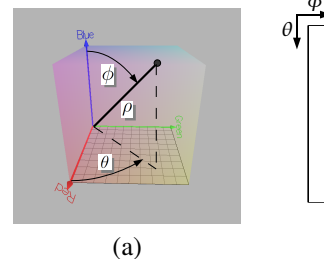
While gray level sets are extracted along the luminance axis of the RGB space, our color sets have to be designed along each body reflection vector revealed by the image. In a few words, the existing approach [1] first scans the RGB space from the black to the white in order to extract the proper gray sets with their connected components. The chromatic segmentation (definition of the body colors) is achieved in a second stage, locally on each gray set. Here, we detect the body colors once and for all in order to design the sets and lines along the color vectors. It can be summed up in the four following stages:

- 1) color conversion in a spherical frame (ρ,θ,ϕ) , as illustrated by Fig.2(a), in order to facilitate the emergence of the body colors. For achromatic colors (on the luminance axis), ρ is directly equivalent to the intensity. For chromatic colors, it is related to the location of ${\bf c}$ on its corresponding body color vector. For a given ρ , (θ,ϕ) are the coordinates of the color located on the spherical surface of distance ρ to the origin;
- 2) extraction of the body colors and body vectors. That is the critical stage of the algorithm, described in Section 3.2;
- 3) classification of the colors to the nearest body vector;
- 4) design of the level sets and lines along each body vector.

It has been shown in [1] that dichromatic lines were robust to angular and spherical color changes.

3.2. Computation of the body colors

In the spherical frame (ρ,θ,ϕ) , the bidimensional histogram $H(\theta,\phi)$ refers to the distribution of the colors independently from their value ρ . Logically, a large density of colors in that histogram is likely to reveal a body vector. As an example, Fig.2(b) shows the histogram of the image PARROTS, where the extrema of the four main body vectors appear. Therefore, these colors could be determined by detecting the local *maxima* in $H(\theta,\phi)$. However, because of noise and because of



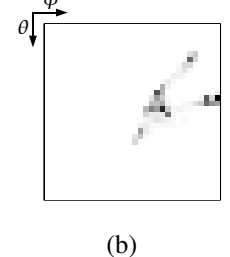


Fig. 2. (a) Spherical representation of the body vector in the RGB cube. (b) Example of histogram $H_{\mathcal{E}}(\theta,\phi)$ of the image PARROTS.

the lambertian approximation, a more appropriate and robust approach has to be designed.

The body colors, *i.e.* the upper (clearer) ends of the body vectors, are extracted in a top-down approach with decreasing values of ρ . In other words, the clear colors are extracted before the dark ones. Let be $H_{\mathcal{E}}(\theta,\phi)$ the 2D histogram of the color components (θ,ϕ) of distance $\rho \geq \mathcal{E}$ from the black. First, the local *maxima* are detected in $H_{\mathcal{E}}(\theta,\phi)$, beginning with the highest value of \mathcal{E} . Since detecting 2D local *maxima* could be too restrictive and yield a low number of *maxima*, we consider the union of the one-dimensional local *maxima* defined on θ and ϕ separately. They form several connected components, called *color signatures* with labels $n_{\mathcal{E}}$. Each $n_{\mathcal{E}}$ is considered as a potential body color of level \mathcal{E} . In a second stage, $H_{\mathcal{E}-1}(\theta,\phi)$, *i.e.* the histogram at lower level (or lower iso-distance to the black), is analyzed similarly, providing a set of labels $n_{\mathcal{E}-1}$.

From one histogram $H_{\mathcal{E}}(\theta,\phi)$ to the other $H_{\mathcal{E}-1}(\theta,\phi)$, the relationship between labels can be described through the two-dimensional *Transition table* $T(n_{\mathcal{E}},n_{\mathcal{E}-1})$. As illustrated on Fig. 3, it is defined in the following way. $T(n_{\mathcal{E}},n_{\mathcal{E}-1})=1$ when at least one bin $H_{\mathcal{E}}(\theta,\phi)$ of label $n_{\mathcal{E}}$ gets a new label $n_{\mathcal{E}-1}$ in the histogram $H_{\mathcal{E}-1}(\theta,\phi)$. Inversely, $T(n_{\mathcal{E}},n_{\mathcal{E}-1})=0$ when none of the labels $n_{\mathcal{E}}$ gets the label $n_{\mathcal{E}-1}$.

Through this table, four phenomena can be detected. 1. Occurrence of a new body color. A new color of label $n_{\mathcal{E}-1}$ is detected when $T(0,n_{\mathcal{E}-1})=1$ and $\forall n_{\mathcal{E}}\neq 0$, $T(n_{\mathcal{E}},n_{\mathcal{E}-1})=0$. That is illustrated in Fig. 3 by the occurrence of the label f, which is consequently considered as a body color.

- **2. Evolving** (i.e expansion, reduction or constancy of a signature). There is an evolving of the signature $n_{\mathcal{E}-1}$ if there is one and only one label $n_{\mathcal{E}} \neq 0$ for which $T(n_{\mathcal{E}}, n_{\mathcal{E}-1}) = 1$. For example, labels b and g correspond finally to the same body vector the end of which has been labeled with value b, and g finally inherits the label b.
- **3. Fusion**. This phenomenon can occur often since the segments become more and more difficult to distinguish when they are close to the origin. Considering one label $n_{\mathcal{E}-1}$, a fusion is detected when there are several $n_{\mathcal{E}}$ for which $T(n_{\mathcal{E}}, n_{\mathcal{E}-1}) = 1$. That is the case of labels c and d which

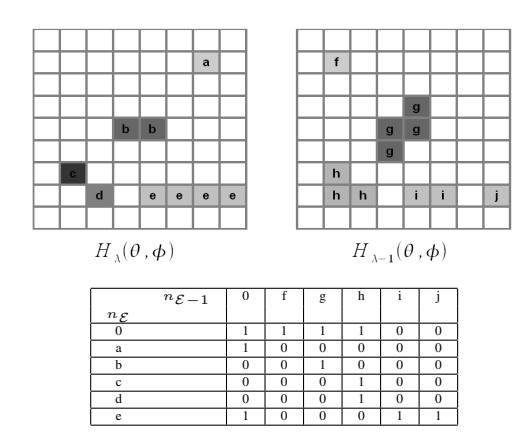


Fig. 3. The Transition Table. (a) Histograms at two successive levels $H_{\mathcal{E}}(\theta,\phi)$ and $H_{\mathcal{E}-1}(\theta,\phi)$, with their color signatures labeled from a to j. (b) Their related transition table, the row entries are the colors signatures $n_{\mathcal{E}}$ while the column entries correspond to the labels $n_{\mathcal{E}-1}$.

are finally fused in one label h. In that case, the colors c and d are considered to be two different body colors, while h is not taken into account.

4. Division. It is a rare phenomenon, which is due to noise, artifacts, and to the limitations of the lambertian assumption. Considering one signature of label $n_{\mathcal{E}}$, a division is detected when, for several $n_{\mathcal{E}-1}$, we have $T(n_{\mathcal{E}}, n_{\mathcal{E}-1}) = 1$. For example, the signature e is replaced by two labels h and i, which will be considered as two different body colors.

Thus, each histogram $H_{\mathcal{E}}(\theta,\phi)$ is processed in the same way, leading finally to the set of the main body colors conveyed by the image.

Once all the levels $\mathcal E$ have been analyzed, one body color $\mathbf c_{\mathbf b}{}^i$ for $i=1..N_c$ has to be associated to each of the N_c distinguished labels. For each color signature, the final body color is chosen as the couple (θ,ϕ) for which $H(\theta,\phi)$ is maximum in the connected component.

3.3. Body sets and lines

Once the body colors and vectors have been determined, each pixel p is projected onto the nearest vector. Then, each vector is divided into upper or lower level sets of ρ . Thus, our approach computes the body color in a more global fashion than as in [1], providing a larger reduction of the number of colors. Here, we require the analysis on one histogram per level instead of one histogram per connected component of the image [1].

4. EXPERIMENTS

Our topographic map is compared to the existing techniques [6, 1]. We call A, B the methods proposed by [6] and [1] respectively, and C refers to the proposed technique. Two quantization levels N_l (8 and 16) are tested 1 .

We define the best collection of level sets as the one which reconstruct the image at best with the lowest number of level sets N_{sets} and within a reasonable executing times. The dissimilarity between the reconstructed image – *i.e.* the collection of color sets– with the original image is evaluated by 2 criteria: the PSNR and the psycho-visual distance CIELAB distance D_{CIE76} (see [10] for instance) with illuminant d_{65} .

Fig. 4 shows the level sets and lines from image PARROTS with $N_l=8$. The method A has produced some false colors, on the yellow feathers and on the leaves for example. B produces less artifacts, but the colors are visually different from the input image (see Fig.1). Finally, our sets seems more faithful to the original, in terms of colors. Let us focus on the color lines, especially in the two boxes. A obviously produces a larger number of lines, globally more tortuous than B and C. The latter produces less lines, which are visually smoother. These results are confirmed by the comparison criteria collected in table 1. Indeed, C provides a lower number of sets and shows the best quality results, i.e. the lowest $D_{CIE_{76}}$ distance and the highest PSNR.

 Table 1. Qualitative results computed on the PARROTS image.

		$N_l = 8$			$N_l = 16$	
	N_{sets}	D_{CIE76}	PSNR	N_{sets}	D_{CIE76}	PSNR
A	3406	26,66	14,78	9242	12,52	17,55
В	332	17,0	15,33	1102	8,34	18,90
C	103	14,63	15,64	944	7,99	19,32

Then, the three methods have been compared on 22 images from the Kodak data base², of size 384 x 256 and 98 images from the Middlebury Stereo Datasets³ of size 638 x 555 approximately. Table 2(a) and 2(b) collect the comparison criteria, μ and σ being the average and standard-deviation computed on the whole database. Here also, whatever the quantization level, C exhibits a smaller number of sets and better preserves the color information.

The HSV space leads to a large number of sets, partly due to the production of noisy and irrelevant sets at low saturation, when hue is ill-defined. Besides, the definition of the color sets along the dominant color vectors of the RGB space have been simplified compared to the existing dichromatic lines [1]. Since the computation of the body colors is now more global while being robust thanks to an appropriate scan in the color space, it is less sensitive to local noise.

Executing times. On Kodak images the sizes of which reduced by a factor of two (192×128) , the computation times are in average 6,5s per image [1]. This result has been produced without any specific optimization and using a processor Intel Pentium III Xeon 2266 MHz, 3Go Ram. With the same computer, the proposed technique takes between 0,3s and 1s for an image of size 695 x 555 (depending on the number of

 $^{^1}$ In order to have the same accuracy than method A and B, we have to consider histograms of size $2N_l \times 2N_l$ if local *maxima* are computed in a 3 \times 3 neighborhood.

²http://r0k.us/graphics/kodak/

³The data sets come from http://vision.middlebury.edu/stereo/data/, in scenes2006, scenes2005 and scenes2003, images disp1.png and disp5.png

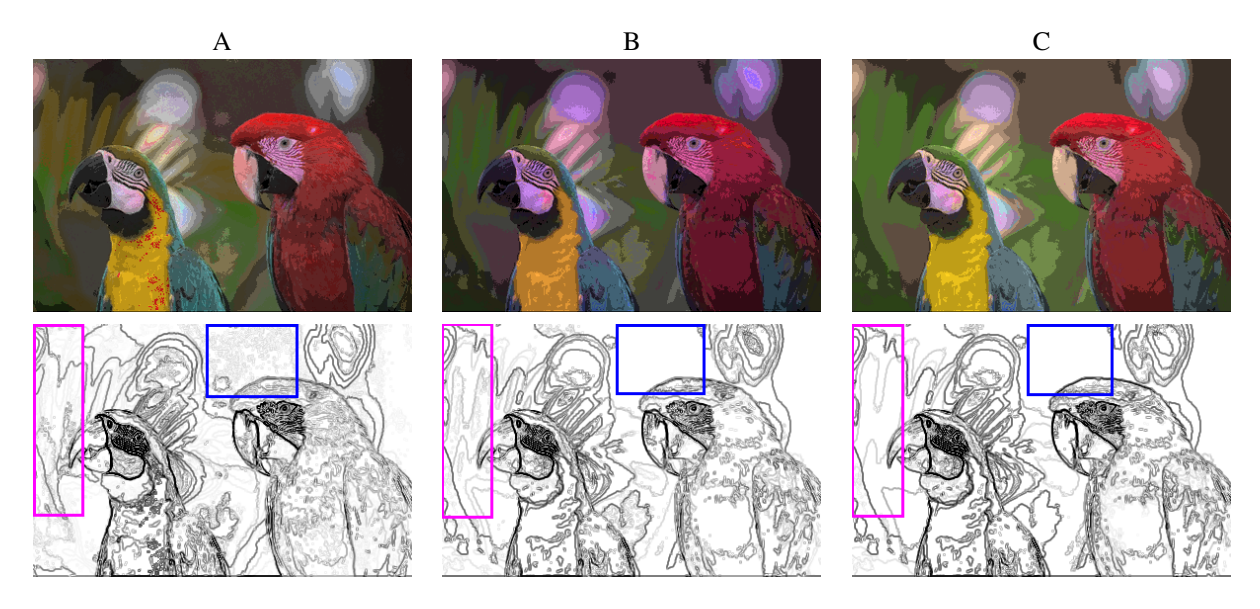


Fig. 4. Color sets (first row) and lines (second row) obtained on the image SYNTHETIC for 8 levels.

Table 2. Quantitative results computed on 120 images for: (a) 8 levels and (b) 16 levels. (μ : average, σ : standard-deviation).

	A 7				DCMD					
	N_{sets}		D_{CIE76}		PSNR					
	μ	σ	μ	σ	μ	σ				
A	5432,7	3706,2	31,07	13,80	17,55	4,33				
В	531,2	231,7	33,34	4,20	18,98	4,73				
C	261,4	276,0	15,10	3,18	20,69	5,09				
(a)										
	N_{sets}		D_{CIE76}		PSNR					
	μ	σ	μ	σ	μ	σ				
Α	18165,9	125016	1 4 57							
Λ	18103,9	13584,6	14,57	5,70	21,14	4,47				
B	8364,9	13584,6 6254,9	14,57	5,70 2,56	21,14 22,12	4,47 4,67				
	1		1 '	´						

colors N_b). Unfortunately, our approach is more time consuming than the total order in HSV, which does not requires any histogram analysis. That is the price to pay to get a more compact representation of the image.

5. CONCLUSION

We have proposed a novel color topographic map based on the lambertian assumption of the dichromatic model. The main body colors are automatically determined and the level sets and lines are extracted along the body vectors. Thus, colors are partially ordered in the RGB space. The computation of the body colors has been achieved *via* the analysis of the multi-level 2D histograms and the introduction of the Transition Table. The experiments have shown that this method yields a good trade-off between compactness and

quality, within reasonable computation times. It overcomes the main defect of HSV representations, the ill-definition of hue for low saturation, which produces irrelevant sets. The data reduction towards a few robust features is likely to reduce the complexity of the downstream algorithms, matching or tracking for instance. That is our present challenge. The proposed method can also be useful for compression purposes or color reduction.

6. REFERENCES

- [1] M. Gouiffès and B. Zavidovique, "A color topographic map based on the dichromatic reflectance model.," *Eurasip Journal On Im. and Video Proc.*, 2008.
- [2] V. Caselles, B. Coll, and J-M. Morel, "Topographic maps and local contrast change in natural images," *IJCV*, vol. 33, no. 1, pp. 5–27, 1999.
- [3] F. Cao, P. Musé, and F. Sur, "Extracting meaningful curves from images," *Journ. of Math. Im. and Vis.*, vol. 22, no. 2, pp. 159–181, 2005.
- [4] C. Ballester, V. Caselles, L. Igual, and L. Garrido, "Level lines selection with variational models for segmentation and encoding," *Journ. of Math. Im. and Vis.*, vol. 27, no. 1, pp. 5–27, 2007.
- [5] S. Bouchafa and B. Zavidovique, "Efficient cumulative matching for image registration," *Im. and Vis. Comp.*, vol. 24, pp. 70–79, 2006.
- [6] B. Coll and J. Froment, "Topographic maps of color images," in 15th Int. Conf. ICPR, 2000.
- [7] V. Caselles, B. Coll, and J-M. Morel, "Geometry and color in natural images," *Journ. of Math. Im. and Vis.*, vol. 16, no. 2, pp. 89–105, 2002.
- [8] S.A. Shafer, "Using color to separate reflection components," Color Research and Applications, vol. 10(4), pp. 210–218, 1985.
- [9] S.K. Nayar, X. Fang, and B. Terrance, "Separation of reflection components using color and polarization," *International Journal of Computer Vision*, vol. 21, no. 3, pp. 163–186, 1997.
- [10] A. Trémeau, C. Fernandez-Maloigne, and P. Bonton, *Image numérique couleur: de l'acquistion au traitement*, Dunod, 2004.